

# Compressed Sensing MRI

1

Michael Lustig, *Student Member, IEEE*, David L. Donoho *Member, IEEE*

Juan M. Santos *Member, IEEE*, and John M. Pauly, *Member, IEEE*

## Abstract

Compressed sensing (CS) aims to reconstruct signals and images from significantly fewer measurements than were traditionally thought necessary. Magnetic Resonance Imaging (MRI) is an essential medical imaging tool burdened by an inherently slow data acquisition process. The application of CS to MRI has the potential for significant scan time reductions, with benefits for patients and health care economics.

MRI obeys two key requirements for successful application of CS: (1) medical imagery is naturally *compressible* by sparse coding in an appropriate transform domain (e.g., by wavelet transform); (2) MRI scanners naturally acquire samples of the *encoded image in spatial frequency*, rather than direct pixel samples.

In this paper we review the requirements for successful CS, describe their natural fit to MRI, and then give examples of four interesting applications of CS in MRI. We emphasize an intuitive understanding of CS by describing the CS reconstruction as a process of interference cancellation. We also emphasize an understanding of the driving factors in applications, including limitations posed by MRI hardware, the characteristics of different types of images, and clinical concerns.

## I. INTRODUCTION

CS is rapidly attracting interest in medical imaging research, and in particular the MRI research community. Although the early theoretical publications on CS appeared quite recently (2006) in journals such as *IEEE Trans. Info. Theory* [1], [2], the idea was already a very visible presence at the Annual

This work was supported by NIH grants P41 RR09784, R01 HL074332, R01 HL075803 and GE Helthcare.

The corresponding author [mlustig@mrsrl.stanford.edu](mailto:mlustig@mrsrl.stanford.edu).

M. Lustig , J. M Santos and J. M. Pauly are with the Magnetic Resonance Systems Research Laboratory, Department of Electrical Engineering, Stanford University, Stanford, CA 94305.

D. L. Donoho is with the Statistics Department, Stanford University, Stanford, CA 94305.

meeting of the International Society for Magnetic Resonance in Medicine in May 2007. The enthusiasm of MRI researchers for CS is driven by two factors. First, MRI is very well suited to CS. The assumptions behind the theory are easy to justify in MRI. Second, the proposed applications offer very significant benefits in imaging speed, which will improve patient care and reduce costs.

This paper presents a basic understanding of the natural fit between MRI and CS and four interesting applications of CS in MRI. In Section II, we review briefly the principles of MRI. We describe how MRI allows efficient sampling of imagery, not in the original spatial domain of pixels or voxels, but instead in an encoded form: samples are acquired along curves in the spatial frequency domain. In Section III we review the natural compressibility of medical images, which can often be represented very efficiently using a relatively small number of coefficients in an appropriate transform domain, such as the wavelet domain. In Section IV we review the requirements for successful use of CS. We describe in particular the notion of incoherence between the frequency domain, where the measurements take place and the sparsification domain, where the signal has a sparse representation. Incoherence allows reconstruction from CS measurements by a very intuitive scheme similar to successive interference cancellation in adaptive signal processing.

Achieving incoherence is the key challenge in designing CS data acquisition methods in MRI; the other requirements are relatively straightforward to meet. The degree of coherence depends on the trajectory in spatial frequency space and on the sparsification domain; good trajectory choice is application-dependent. Section V discusses four interesting applications: Rapid Contrast-Enhanced 3D Angiography, Whole-Heart Coronary Imaging, Brain Imaging, and Dynamic Heart Imaging. These different applications require varying choices of sparsification domains and sampling trajectories; the choices are driven by instrumental considerations, image characteristics and the imaging paradigm. We review these factors and describe how they drive the design decisions in each application.

## II. PRINCIPLES OF MAGNETIC RESONANCE IMAGING

This section briefly sketches the MRI concepts needed for an electrical engineer with a signal processing background to understand the features of MRI related to CS. More complete descriptions of MRI can be found in the excellent survey paper by Wright [3] that appeared in this magazine, and the many MRI textbooks [4]–[6].

### A. Nuclear Magnetic Resonance Physics

The MRI signal is generated by protons in the body, mostly those in water molecules. A strong static field  $B_0$  (See Fig. 1) polarizes the protons, yielding a net magnetic moment oriented in the direction of the static field. Applying a radio frequency (RF) excitation field  $B_1$  (See Fig. 1) to this net magnetization tips it and produces a magnetization component  $m$  transverse to the static field. The magnetization precesses at characteristic frequency

$$f_0 = \frac{\gamma}{2\pi} B_0.$$

Here  $f_0$  denotes the precession frequency,  $B_0$  the static field strength, and  $\gamma/2\pi$  is a constant (42.57 MHz/T) [6]. A typical 1.5T clinical MR system has a frequency of about 64 MHz. The transverse component of the precessing magnetization produces a signal detectable by a receiver coil. The transverse magnetization at a position  $r$  is represented by the complex quantity  $m(r) = |m(r)| \cdot e^{-i\phi(r)}$ , where  $|m(r)|$  is the magnitude of the transverse magnetization and  $\phi(r)$  is its phase. The phase indicates the direction the magnetization is pointing in the transverse plane. The transverse magnetization  $m(r)$  can represent many different physical properties of tissue. One very intuitive property is the proton density of the tissue, but other properties [7] can be emphasized as well. The MR image we are interested in is  $m(r)$ , depicting the spatial distribution of the transverse magnetization. Next, we will review how to resolve that spatial distribution.

### B. Spatial Encoding

MR systems can encode spatial information in the MR signal by superimposing additional magnetic fields on top of the strong static field. These fields vary linearly in space and therefore are called *gradient fields* (see Fig. 1), they are denoted as  $G_x$ ,  $G_y$  and  $G_z$  corresponding to the three Cartesian axes. As an example, when  $G_x$  is applied, the magnetic field will vary with position as  $B(x) = B_0 + G_x x$ . This variation causes the precession frequency to vary linearly in space,

$$f(x) = \frac{\gamma}{2\pi} (B_0 + G_x x).$$

As a result, magnetization at positive  $x$  positions will precess at a higher frequency than magnetization at negative  $x$  positions.

Spatial encoding using gradients can be understood by a musical instrument analogy: the piano. The pitch of a piano note varies linearly with the position of the key being struck; the sound one hears is

the net sum of all notes emitted. A skilled musician listening to the emitted polyharmonic sound can hear which notes are playing and say which keys were pressed (and how strongly). The MR signal generated in the presence of a gradient field is likewise a polyphonic mixture. The spatial positions within the patient's body are like piano keys and the emitted RF signal from each position is like a "note," with a frequency linearly varying with position. The polyharmonic MR signal superimposes the different "notes;" they encode the spatial position and the magnetization strength at those positions. A signal processing engineer can immediately realize the Fourier relation between the received MR signal and the magnetization distribution, and that the magnetization distribution can be decoded by a spectral decomposition.

To see this Fourier relation more concretely consider the following: the gradient-induced variation in precession frequency causes a location dependent phase dispersion to develop. The additional frequency contributed by gradient fields can be written as

$$f(r) = \frac{\gamma}{2\pi} G(t) \cdot r,$$

where  $G(t)$  is a vector of the gradient fields amplitudes. The phase of magnetization is the integral of frequency starting from time zero (immediately following the RF excitation):

$$\begin{aligned} \phi(r, t) &= 2\pi \int_0^t \frac{\gamma}{2\pi} G(s) \cdot r ds \\ &= 2\pi r \cdot k(t), \end{aligned}$$

where

$$k(t) \equiv \frac{\gamma}{2\pi} \int_0^t G(s) ds.$$

The receiver coil integrates over the entire volume, producing a signal

$$s(t) = \int_R m(r) e^{-i2\pi k(t) \cdot r} dr.$$

This is the *signal equation for MRI*. In words, the received signal at time  $t$  is the Fourier transform of the object  $m(r)$  sampled at the spatial frequency  $k(t)$ . Such information is fundamentally encoded and very different than traditional optical imaging where pixel samples are measured directly.

The design of an MRI acquisition method centers on developing the gradient waveforms  $G(t)$  that drive the MR system. These waveforms, along with the associated RF pulses used to produce the magnetization, are called a *pulse sequence*. The integral of the  $G(t)$  waveforms traces out a trajectory  $k(t)$  in spatial frequency space, or  $k$ -space. For illustration, consider the simple example in Fig. 2 where, immediately

after the RF excitation, a  $G_x$  gradient field is applied followed by a  $G_y$  gradient. The phases of the magnetization are shown at different time points, along with the  $k$ -space trajectory and the MR signal. This encoded sampling and the freedom in choosing the sampling trajectory play a major role in making CS ideas naturally applicable to MRI.

### C. Image Acquisition

Constructing a single MR image commonly involves collecting a series of frames of data, called *acquisitions*. In each acquisition, an RF excitation produces new transverse magnetization, which is then sampled along a particular trajectory in  $k$ -space.

In principle, a complete MR image can be reconstructed from a single acquisition by using a  $k$ -space trajectory that covers a whole region of  $k$ -space [8]. This is commonly done in applications such as imaging brain activation. However, for most applications this results in inadequate image resolution and excessive image artifacts.

Magnetization decays exponentially with time. This limits the useful acquisition time window. Also, the gradient system performance and physiological constraints limit the speed at which  $k$ -space can be traversed (See Fig. 2). These two effects combine to limit the total number of samples per acquisition. As a result, most MRI imaging methods use a sequence of acquisitions; each one samples part of  $k$ -space. The data from this sequence of acquisitions is then used to reconstruct an image.

Traditionally the  $k$ -space sampling pattern is designed to meet the Nyquist criterion, which depends on the resolution and field of view (FOV) as shown in Fig. 3. Image resolution is determined by the sampled region of  $k$ -space: a larger region of sampling gives higher resolution. The supported field of view (FOV) is determined by the sampling density within the sampled region: larger objects require denser sampling to meet the Nyquist criterion. Violation of the Nyquist criterion causes the linear reconstruction to exhibit artifacts. The appearance of such artifacts depends on the details in the sampling pattern, as discussed below.

In MRI, it is possible to selectively excite a thin slice through the three dimensional volume. This reduces the data collection to two dimensions in  $k$ -space for each slice. The volumetric object is imaged by exciting more slices, known as a multi-slice acquisition. When a volume or a thick slab is excited, a 3D  $k$ -space volume must be sampled. Each of these approaches is very common, and has advantages in specific applications [4]–[6].

We have considerable freedom in designing the  $k$ -space trajectory for each acquisition. Some 2D and

3D sampling trajectories are illustrated in Fig. 4. By far the most popular trajectory uses straight lines from a Cartesian grid. Most pulse sequences used in clinical imaging today are Cartesian. Reconstruction from such acquisitions is wonderfully simple: apply the inverse Fast Fourier Transform (FFT). More importantly, reconstructions from Cartesian sampling are robust to many sources of system imperfections.

While Cartesian trajectories are by far the most popular, many other trajectories are in use, including sampling along radial lines and sampling along spiral trajectories. Radial acquisitions are less susceptible to motion artifacts than Cartesian trajectories [9], and can be significantly undersampled [10], especially for high contrast objects [11], [12]. Spirals make efficient use of the gradient system hardware, and are used in real-time and rapid imaging applications [13]. Reconstruction from such non-Cartesian trajectories is more complicated, requiring filtered back-projection algorithms [14] or  $k$ -space interpolation schemes (e.g. gridding [15]).

#### *D. Rapid Imaging*

MR acquisition is inherently a process of traversing curves in multi-dimensional  $k$ -space. The speed of  $k$ -space traversal is limited by physical constraints. In current systems, gradients are limited by maximum amplitude and maximum slew-rate (See Fig. 2. In addition, high gradient amplitudes and rapid switching can produce peripheral nerve stimulation in patients [16]. Since this must be avoided, the physiology of the patient provides a fundamental limit to gradient system performance.

Because sampling speed is fundamentally limited, many researchers are striving to reduce the amount of acquired data without degrading image quality. Many such efforts are inspired by the idea that MRI data are, or can be made to be, redundant. Such redundancy can be created by design, for example, using multiple receiver coils [17], [18], which provides more useful data per MR acquisition, so fewer acquisitions are needed per scan. Redundancy can be a known or modeled signal property such as spatial-temporal correlation [19]–[26] or a redundancy learned and extracted from the data itself [27]–[29].

All efforts at reduced data acquisition might well be labeled “compressive sampling,” however, the underlying phenomena being exploited are often quite different. In this paper, we focus on approaches rooted in the theory described in [1], [2]; such approaches are called here CS approaches. Much ongoing work is based on such approaches [30]–[37].

### III. THE SPARSITY/COMPRESSIBILITY OF MR IMAGES

Natural images can often be compressed with little or no perceptible loss of information [38]. The world-wide-web demonstrates this billions of times weekly. Medical images are just as compressible [39] as other imagery, although historically compression has been avoided in medical applications [40].

Transform-based compression is a widely used compression strategy adopted in the JPEG, JPEG-2000, and MPEG standards. This strategy first applies a sparsifying transform, mapping image content into a vector of sparse coefficients, and then encodes the sparse vector by approximating the most significant coefficients and ignoring the smaller ones. The Discrete Cosine transforms (DCT) is the sparsifying transform at the heart of JPEG, while the discrete wavelet transform (DWT) is the workhorse of JPEG-2000, respectively [38].

Most MR images are sparse in an appropriate transform domain. To begin with, consider angiograms, which are images of blood vessels in the body. These images contain primarily contrast-enhanced blood vessels in a sea of void and look sparse to the naked eye. Equivalently, they are already sparse in the pixel domain, so here the sparsifying transform is the identity transform. Some brain images are piecewise smooth and their gradient field is sparse; the sparsifying transform there is spatial finite-differencing. More complex imagery can be sparsified in more sophisticated domains, such as the discrete cosine transform domain or the wavelet domain – witness the success of JPEG and JPEG-2000, respectively.

Sparse representation is not limited to still imagery. Many still images can be compressed 5 to 10-fold without perceptible loss of visual information, but often videos can safely be compressed much more heavily. This is demonstrated by the success of MPEG, which uses the fact that some parts of a movie are either constant or else undergo motion that is similar between neighboring pixels. Interframe temporal differences of video content are often sparse, so movies are sparsified by temporal finite differences. Dynamic MR images are highly compressible as well. For example, heart images are quasi-periodic. Therefore, their temporal Fourier transform is sparse. The hemodynamic response of brain activation in some functional MRI experiments can also be sparsified by temporal Fourier transform.

The transform sparsity of MR images can be demonstrated by applying a sparsifying transform to a conventional MR image and reconstructing an approximation to the image using a subset of the largest transform coefficients. To illustrate this, consider Fig. 5 in which a typical brain image was compressed with wavelets, a slice of an angiogram was compressed with finite-differences, and the time series of a cross section of a dynamic heart sequence was compressed by temporal Fourier transform. The important

information is captured by 10%, 5% and 5% of the largest transform coefficients, respectively.

Uncovering transform sparsity in the context of CS offers a research challenge to the signal processing community. As we will see, it is not enough to identify a sparse representation: the sparsifying transform must also be incoherent with respect to the sampling transform.

#### IV. THE NATURAL FIT BETWEEN CS AND MRI

The transform sparsity of MR images and the coded nature of MR acquisition are two key properties enabling CS in MRI. Figure 6 illustrates these elements, making MRI a natural CS system. We now give a more formal discussion of the requirements.

##### A. Compressed Sensing Theory

CS emerged in the literature of Information Theory and Approximation Theory as an abstract mathematical idea [1], [2]. One measures a relatively small number of ‘random’ linear combinations of the signal values – much smaller than the number of signal samples nominally defining it. However, because the underlying signal is compressible, the nominal number of signal samples is a gross over-estimate of the ‘effective’ number of ‘degrees of freedom’ of the signal. As a result, the signal can be reconstructed with good accuracy from relatively few measurements by a non-linear procedure.

In MRI, we look at a special case of CS where the sampled linear combinations are simply individual Fourier coefficients ( $k$ -space samples). In that setting, CS is claimed to be able to make accurate reconstructions from a small subset of  $k$ -space, rather than an entire  $k$ -space grid.

Theoretical and technical aspects of CS are discussed elsewhere in this special issue. However, the key points can be reduced to nontechnical language. A successful application of CS requires:

- CS1 **Transform Sparsity:** The desired image must have a sparse representation in a known transform domain (i.e., it must be compressible by transform coding),
- CS2 **Incoherence of Undersampling Artifacts:** The aliasing artifacts in a linear reconstruction caused by  $k$ -space undersampling must be incoherent (noise-like) in the sparsifying transform domain.
- CS3 **Nonlinear Reconstruction:** The image must be reconstructed by a non-linear method which enforces both sparsity of the image representation and consistency of the reconstruction with the acquired samples.

The first condition is clearly met for MR images, as explained in Section III above. The fact that incoherence is important, that MR acquisition can be designed to achieve incoherent undersampling, and the fact that there are efficient and practical algorithms for reconstruction will not, at this point in the article, be at all obvious. So we turn to a very simple example.

### *B. Intuitive example: Interference Cancellation*

To develop intuition for the importance of incoherence and the feasibility of CS, consider the 1D case illustrated in Fig. 7. A sparse signal (Fig. 7.1), is sub-Nyquist (8-fold) sampled in  $k$ -space (Fig. 7.2). A textbook linear reconstruction simply zero-fills the missing  $k$ -space values and inverts the Fourier transform; this produces artifacts which depend on the type of undersampling, i.e. which  $k$ -space values are sampled and which are not sampled, and the signal energy distribution in the frequency domain. While equispaced undersampling is a standard topic in signal processing classes, this is inherently a bad scheme to use here. With equispaced undersampling (Fig. 7.3a), this reconstruction generates a superposition of shifted signal copies. In this case, recovery of the original signal is hopeless, as each replica is an equally likely candidate.

With random undersampling, the situation is very different. The zero-filled Fourier reconstruction exhibits incoherent artifacts that actually behave much like additive random noise (Fig. 7.3). Despite appearances, the artifacts are not noise; rather, undersampling causes leakage of energy away from each individual nonzero value of the original signal. This energy appears in other reconstructed signal coefficients, including those which had been zero in the original signal.

It is possible, starting from knowledge of the  $k$ -space sampling scheme and the underlying original signal, to calculate this leakage analytically. This observation immediately suggests a nonlinear iterative technique which enables accurate recovery, even though the signal in Fig. 7.1 was 8-fold undersampled.

The recovery procedure is illustrated in Figs. 7.4-7. Because the signal to be recovered is sparse, it has a few truly nonzero values in a “sea” of zeros. The zero-filled Fourier reconstruction will look like a noisy version of the signal (Fig. 7.4). Again this “noise” is not random noise, but is interference caused by the signal we are trying to recover. When the signal to be recovered is smaller, the interference level will also be smaller. The largest true nonzeros in the original sparse signal will stand out above the level of the interference, although some true nonzeros may be submerged beneath it. By setting an appropriate threshold, the largest components can be detected (Fig. 7.5.), while most values which were truly zero in the original signal will not rise above threshold.

Next we introduce the idea of iteration. The interference caused by the already-detected components can be calculated analytically by assuming that the original signal consisted only of those few detected values (Fig.7.6.). Once computed, the calculated interference can be subtracted away. This yields a new reconstruction which still looks noisy, but in which the noise attributed to interference caused by the largest few nonzeros has been eliminated (Fig. 7.7.). The total interference level is thus reduced. If we now set a new threshold based on this lower level of interference, some of the truly nonzero values in the original sparse signal are now higher than the interference level, and can now be successfully detected. In our example, this procedure is repeated until all the significant signal components are recovered. A recovery procedure along the lines just described was proposed in [41] as a fast approximate algorithm for CS reconstruction.

### *C. Incoherent Sampling in MRI*

Designing a CS scheme for MRI can now be viewed as selecting a subset of the frequency domain which can be efficiently sampled, and is incoherent with respect to the sparsifying transform.

Before we formally introduce the notion of incoherence, we note that narrow optimization of incoherence must not be pushed too far. Some of the most powerful and elegant results about CS have been obtained for sampling a completely random subset of  $k$ -space, which indeed gives very low coherence [1]. The motivation for random sampling can be easily and intuitively understood using our 1D example given earlier in subsection IV-B. Although random sampling is an inspiring and instructive idea, sampling a truly random subset of  $k$ -space is generally impractical; it can be far slower than conventional Nyquist rate sampled Cartesian MRI. Any practical sampling trajectory must satisfy hardware and physiological constraints. Therefore sampling trajectories must follow relatively smooth lines and curves. Sampling schemes must also be robust to non-ideal, real-life situations. Non-Cartesian sampling schemes are often sensitive to magnetic field homogeneity, eddy currents, signal decay, hardware delays and other sources of imperfection.

Furthermore, a uniform random distribution of samples in spatial frequency does not take into account the energy distribution of MR images in  $k$ -space, which is far from uniform. Most of energy in MR imagery is concentrated close to the center of  $k$ -space and rapidly decays towards the periphery of  $k$ -space.

Therefore, realistic designs for CS in MRI should have variable-density sampling with denser sampling near the center of  $k$ -space, matching the energy distribution in  $k$ -space. Such designs should also create

$k$ -space trajectories that are somewhat irregular and partially mimic the incoherence properties of pure random sampling, yet allow rapid collection of data. To compare designs, we need a quantitative notion of incoherence that will allow us to compare data acquisition schemes and their performance.

### *Measuring Incoherence*

We first measure incoherence for cases where the image is already sparse in the pixel domain, so no further sparsification is needed. Suppose we sample a subset  $S$  of  $k$ -space. Let  $\mathcal{F}_S$  denote the Fourier transform evaluated just at frequencies in subset  $S$ . Let  $\mathcal{F}_S^*$  denote the adjoint operation, which can be represented as zero-filling followed by inverse Fourier transform. Define the *point spread function* (PSF) as, simply  $PSF(i, j) = (\mathcal{F}_S^* \mathcal{F}_S)(i, j)$ . Under complete Cartesian sampling, the PSF is the identity and off-diagonal terms vanish. Undersampling  $k$ -space induces nonzero off-diagonal terms in  $PSF(i, j)$ . A nonzero at  $(i, j)$  means that linear reconstruction of pixel  $i$  suffers interference by a unit impulse in pixel  $j \neq i$ . In short, the PSF measures the tendency of zero-filled linear reconstruction to leak energy from the true underlying source pixel to other pixels. This energy shows up as blurring or aliasing artifacts in the image (See Fig. 8 for examples). The goal of irregular sampling is to spread such leakage quasi-uniformly across the image, so that the maximal leakage is small. Accordingly, we define coherence as the maximum off-diagonal entry in a properly normalized PSF. This is analogous to notions of sidelobe-to-peak ratio the reader will have encountered in many branches of signal processing.

Most MR images are sparse in a transform domain other than the pixel domain. In such settings, we use the notion of the *transform point spread function* (TPSF). Let  $\Psi$  denote the sparsifying transform; and then define  $TPSF(i, j) = (\Psi^* \mathcal{F}_S^* \mathcal{F}_S \Psi)(i, j)$ . With this notation, coherence is formally measured by

$$\max_{i \neq j} |TPSF(i, j)|,$$

the maximum size of any off-diagonal entry in the TPSF. Small coherence, e.g. incoherence, is desirable. More discussion about the TPSF can be found in [30].

### *Incoherent MRI Acquisition*

We now consider several schemes and their associated coherence properties. In 2D Cartesian MRI, complete Cartesian sampling is often implemented as a series of  $n_{pe}$  acquisitions (called *phase encodes*) along very simple trajectories: parallel equispaced lines. This scheme yields, say,  $n_{fe}$   $k$ -space samples

per trajectory (called *frequency encodes*), producing a Cartesian grid of  $n_{pe} \times n_{fe}$  samples overall. The sampling along a trajectory, e.g. the frequency encodes, are rarely a limiting factor in terms of sampling-rate and in terms of the scan time. The number of acquisition lines, e.g. the phase encodes, is limiting.

This suggests immediately to speed up a whole scan by simply dropping entire lines from an existing complete grid. This is indeed practical: one has complete freedom in choosing the lines to acquire, and the number of lines is what determines the overall scan time, so scan time reduction is exactly proportional to the degree of undersampling. In fact, implementation of this scheme requires only minor modifications to existing pulse sequences— simply skip certain acquisitions. Since most pulse sequences in clinical use are Cartesian, it is very convenient to implement a CS acquisition this way.

Undersampling parallel lines suffers a drawback: the achievable coherence is significantly worse than with truly 2D random  $k$ -space sampling. In 2D imaging, only one dimension is undersampled, things behave as if the images were one-dimensional signals and we are randomly sampling the 1D frequency domain exploiting only 1D sparsity. This reduced incoherence is visible in Fig. 8a.

In 3D Cartesian imaging the situation improves. Now, there is an additional encoding dimension (called the *slice encode*). Standard Cartesian collections acquire data from  $n_{se} \times n_{pe}$  parallel equispaced lines with  $n_{fe}$  equispaced samples per line, filling out a complete  $n_{se} \times n_{pe} \times n_{fe}$  grid in  $k$ -space. It is very practical to undersample the set of lines, just as in the 2D case. However, the coherence (in the slice-phase encode cross-section) is much smaller than in a comparable 2D scheme with the same number of  $k$ -space samples (see Fig. 8b). Undersampling parallel lines in 3D has another advantage: real 3D volumetric images have 2D cross-sections which are significantly more compressible than their 1D profiles, so the effectiveness of CS is much higher. 3D Cartesian CS is particularly attractive because 3D imaging is more time-consuming than 2D imaging, so scan time reduction has more impact.

Getting completely away from a Cartesian grid allows far greater flexibility in designing sampling trajectories with low coherence. Popular non-Cartesian schemes include sampling along radial lines or spirals. Traditionally, undersampled radial trajectories have been used [10]–[12] to accelerate acquisitions, because the artifacts from linear reconstruction seem benign and incoherent – much like adding noise to the image. Variable-density spirals [42], [43] and also variable density Cartesian acquisitions [44]–[46] have been proposed for similar reasons. From our perspective, we recognize that such artifacts are benign because *the corresponding PSFs are incoherent*. Figure 8c-f shows the PSF of several such trajectories: radial, uniform spirals, variable density spirals and variable density perturbed spirals. These trajectories are strong candidates for CS: with appropriate nonlinear reconstruction, the seeming noise-like artifacts

can be suppressed without degrading image quality.

A dynamic sequence of images is a multi-dimensional signal with two or three spatial coordinates and time as an additional dimension (See Fig. 9 top-left panel). Dynamic MRI data are acquired in the spatial frequency vs time ( $k - t$ ) domain. Traditional collection schemes sample the  $k - t$  domain on a regular set of congruent lines (Fig. 9 top-right). Often, it is impossible to meet the spatio-temporal Nyquist-rate this way. Then, sub-Nyquist sampling, followed by linear reconstruction, causes coherent aliasing of the signal in the spatial-temporal frequency ( $x - f$ ) domain. As an alternative, randomly ordering a subset of  $k$ -space lines (Fig. 9 bottom-right) is incoherent with respect to the  $x - f$  domain and produces benign artifacts in linear reconstructions [23]. So random ordering of lines is an effective and inexpensive way to incoherently sample dynamic data. Of course, the same ideas of random ordering apply to non-Cartesian sampling such as radial lines and spirals, improving incoherence and better exploiting the hardware.

Dynamic imaging CS has major advantages over static imaging: sequences of images, like videos, are highly compressible – much more than static images as illustrated in both Figs. 5 and 9 bottom-left panel. At the same time, dynamic imaging requires several orders of magnitude more samples than static imaging and it is often impossible to meet the Nyquist rate. CS compensates for this by incoherent sampling and by exploiting the inherent sparsity of the dynamic sequence.

#### D. Image Reconstruction

We now briefly describe a useful formal approach for reconstruction. Represent the reconstructed image by a complex vector  $m$ , let  $\Psi$  denote the linear operator that transforms from pixel representation into a sparse representation. Let  $\mathcal{F}_S$  denote the undersampled Fourier transform, corresponding to one of the  $k$ -space undersampling schemes discussed earlier. Our reconstructions are obtained by solving the following constrained optimization problem:

$$\begin{aligned} \text{minimize} \quad & \|\Psi m\|_1 \\ \text{s.t.} \quad & \|\mathcal{F}_S m - y\|_2 < \epsilon, \end{aligned}$$

where  $y$  is the measured  $k$ -space data from the MRI scanner and  $\epsilon$  controls the fidelity of the reconstruction to the measured data. The threshold parameter  $\epsilon$  is roughly the expected noise level. Here the  $\ell_1$  norm  $\|x\|_1 = \sum_i |x_i|$ .

Minimizing the  $\ell_1$  norm of  $\|\Psi m\|_1$  promotes sparsity [47]. The constraint  $\|\mathcal{F}_S m - y\|_2 < \epsilon$  enforces data consistency. In words, among all solutions which are consistent with the acquired data, Eq. 1 finds

a solution which is compressible by the transform  $\Psi$ .

When finite-differences are used for the sparsifying transform, the objective in the optimization is effectively the Total-Variation (TV) [48] norm, a widely-used objective in image processing. Even if another sparsifying transform is intended, it is often useful to include a TV penalty as well [49]–[51]. Such a combined objective seeks image sparsity both in the transform domain and the finite-differences domain, simultaneously. In this case the optimization is written as

$$\begin{aligned} \text{minimize} \quad & \|\Psi m\|_1 + \lambda TV(m) \\ \text{s.t.} \quad & \|\mathcal{F}_S m - y\|_2 < \epsilon, \end{aligned}$$

where  $\lambda$  trades  $\Psi$ -sparsity with finite-differences sparsity.

The reader may well ask how such formal optimization-based reconstructions relate to the informal idea of successive interference cancellation. In fact, iterative algorithms for solving such formal optimization problems in effect perform thresholding and interference cancellation at each iteration so there is a close connection between our exposition and more formal approaches [41], [50], [52], [53].

## V. APPLICATIONS OF COMPRESSED SENSING TO MRI

We now describe four potential applications of CS in MRI: (a) Rapid Angiography; (b) Whole-Heart Coronary Imaging; (c) Enhanced Brain Imaging; (d) Dynamic Heart Imaging.

The three requirements for successful CS in MRI come together differently in different applications. Of particular interest is the way in which different applications face different constraints, imposed by MRI scanning hardware or by patient considerations, and how the inherent freedom of CS to choose sampling trajectories and sparsifying transforms plays a key role in matching the constraints.

### A. Rapid 3D Angiography

Angiography is increasingly popular for diagnosis of vascular disease. It attempts to image blood vessels in the body and helps to detect aneurysms, vascular occlusions, stenotic disease and tumor feeder vessels. It also serves to guide surgical procedures and to monitor the treatment of vascular disease [54]. Often, a contrast agent is injected, significantly increasing the blood signal and enabling rapid data acquisition. In angiography, a significant portion of the diagnostic information comes from imaging the dynamics of the contrast agent bolus. This requires high spatial and temporal resolution with a very large FOV – obviously a very difficult task. Today MR angiography scans are often undersampled [11],

[12], [55] obtaining improved spatial resolution and temporal resolution at the expense of undersampling artifacts.

CS is particularly suitable for angiography. Angiograms are inherently sparse images – already sparse in the pixel representation, and are sparsified even better by spatial finite-differences (See Fig. 5). The need for rapid high temporal and spatial resolution imaging means that undersampling is almost inevitable. CS offers to improve current strategies by significantly reducing the artifacts that result from undersampling.

In this example, we apply CS to 3D Cartesian contrast-enhanced angiography (the most common scheme in clinical practice). Figure 10 illustrates the collection scheme, acquiring equispaced parallel lines in  $k$ -space. Choosing a pseudo-random subset with variable  $k$ -space density of 10% of those lines combines undersampling with low coherence. Fig. 10 shows a maximum intensity projection (MIP) through the 3D volume of several reconstructions. CS is able to significantly accelerate angiography imaging, enabling better temporal resolution or alternatively improving the resolution of current imagery without compromising scan time. The nonlinear reconstruction in CS avoids most of the artifacts that appear in linear reconstruction from undersampled data.

### *B. Whole Heart Coronary Imaging*

X-ray coronary angiography is the gold standard for evaluating coronary artery disease, but it is invasive. Multi-slice x-ray CT is a non-invasive alternative, but generates high doses of ionizing radiation. MRI is emerging as a non-invasive, non-ionizing alternative [13], [56]–[59].

Coronary arteries are constantly subject to heart and respiratory motion; high-resolution imaging is therefore a challenging task. Heart motion can be handled by synchronizing acquisitions to the cardiac cycle (cardiac gating). Respiratory motion can be mitigated by long scans with navigated breathing compensation [59], or simply by short breath-held acquisitions [13], [56]. However, breath-held cardiac-triggered collection schemes face strict timing constraints and very short imaging windows. The number of acquisitions is limited to the number of cardiac cycles in the breath-hold period. The number of heartbeats per period is itself limited – patients in need of coronary diagnosis cannot be expected to hold their breath for long! Also, each acquisition must be very short to avoid motion blurring. On top of this, many slices need to be collected to cover the whole volume of the heart. Because of these constraints, traditionally breath-held cardiac triggered acquisitions have limited spatial resolution and only partial coverage of the heart [56], [59]. Compressed sensing can accelerate data acquisition, allowing the entire heart to be imaged in a single breath-hold [60].

Figure 11 shows a diagram of the multi-slice acquisition. To meet the strict timing requirements, the hardware efficient spiral  $k$ -space trajectory is used. For each cardiac trigger, a single spiral in  $k$ -space is acquired for each slice. The heart does move considerably during the imaging period, but because each acquisition is very short, each slice is relatively immune to motion and inter-slice motion is manifested as geometric distortion across the slices rather than blurring. Geometric distortion has little effect on the clinical diagnostic value of the image. Even though spirals are very efficient, the strict timing limitations make it necessary to undersample  $k$ -space 2-fold. To do so, undersampled variable density spirals [42] are used. Such spirals have an incoherent PSF (see Fig. 8e). When used with linear gridding reconstruction [15] undersampling artifacts are incoherent and appear simply as added noise. Coronary images are generally piece-wise smooth and are sparsified well by finite-differences. CS reconstruction can suppress undersampling-induced interference without degrading the image quality.

Figure 11 shows a comparison of the linear direct gridding reconstruction and CS, on the right coronary artery reformatted from a single breath-hold whole-heart acquisition. The linear gridding reconstruction suffers from apparent noise artifacts actually caused by undersampling. Indeed, the CS reconstruction suppresses those artifacts, without impairing the image quality.

### C. Brain Imaging

Brain scans are the most common clinical application of MRI; most such scans are 2D Cartesian multi-slice. For scan time reasons and SNR reasons, the slices are often quite thick, often with large gaps between slices. The ideas of CS promise to reduce collection time while improving the resolution of current imagery. Indeed, by significantly undersampling the existing  $k$ -space, some of the saved collection time could be used to collect data from the missing slices, and still leave a shorter collection overall. But are the requirements for CS all satisfied? Section III showed that brain images exhibit transform sparsity in the wavelet domain. If incoherence can be obtained, the application may succeed.

We tested the application of CS to brain imaging by acquiring a full Nyquist sampled data-set which we undersampled in retrospect. Our idea was to explore various combinations of scan time reduction and improved resolution.

The 2D Cartesian multi-slice sampling trajectories are illustrated in Fig. 12. For each slice we selected a different random subset of 80 trajectories from 192 possible trajectories – a speedup factor 2.4. Undersampling each slice differently reduces coherence compared to sampling the same way in all slices; see [30].

Figure 12 shows the experimental results. In Fig. 12a coronal and axial slices of the multi-slice CS reconstruction are compared to full Nyquist sampling, linear reconstruction from the undersampled data, and linear reconstruction from a low resolution (LR) acquisition taking the same amount of scan time. CS exhibits both significant resolution improvement over LR at the same scan time, and significant suppression of the aliasing artifacts compared to the linear reconstruction with the same undersampling.

#### D. $k$ - $t$ Sparse: Application to Dynamic Heart Imaging

Dynamic imaging of time-varying objects is challenging because of the spatial and temporal sampling requirements of the Nyquist criterion. Often temporal resolution is traded off against spatial resolution (or vice versa). Artifacts appear in the traditional linear reconstruction when the Nyquist criterion is violated.

Now consider a special case: dynamic imaging of time-varying objects undergoing quasi-periodic changes. Special cases include heart imaging, which we focus on here, but also imaging the hemodynamic response of functional brain activity. Heart motion is quasi-periodic: the time series of intensity in a single voxel is sparse in the temporal frequency domain (See Fig. 5). At the same time, a single frame of the heart ‘movie’ is sparse in the wavelet domain. A simple transform can exploit both effects: apply a spatial wavelet transform followed by a temporal Fourier transform (see Fig. 9 bottom-left panel).

Can we exploit the natural sparsity of dynamic sequences to reconstruct a time-varying object sampled at significantly sub-Nyquist rates? Consider the Cartesian sampling scheme that acquires for each time slice a single line in  $k$ -space, following an orderly progression through the space of lines as time progresses (see Fig. 9 top-right panel). For our desired FOV and resolution it is impossible, using this scheme, to meet the spatial-temporal Nyquist rate. In fact, this scheme is particularly inefficient for dynamic imaging with traditional acquisitions and reconstruction methods. Instead, we make one change: make the  $k$ -space line ordering *random* instead of orderly [23], [32]. The random ordering comes much closer to randomly sampling  $k - t$  space (See Fig. 9 bottom-right panel) and the sampling operator becomes much less coherent with the sparsifying transform.

Fig. 13 shows results from two experiments. The first result used synthetic data: a motion phantom, periodically changing in a cartoon of heart motion. The figure depicts an image sequence reconstructed from a sampling rate 4 times slower than the Nyquist rate, using randomly-ordered acquisition and nonlinear reconstruction. The second result involved dynamic real-time acquisition of heart motion. The given FOV (16cm), resolution (2.5mm) and repetition time (4.4ms) allows a Nyquist rate of 3.6 frames per second (FPS). This leads to temporal blurring and artifacts in the traditionally-reconstructed image.

By instead using random ordering and CS reconstruction we were able to recover the dynamic sequence at the much higher rate of 25FPS with significantly reduced image artifacts.

## VI. RELATION TO OTHER METHODS

Much ongoing development of new MRI methods is concerned with speeding up MRI. CS is complementary to much of this work, and can be used to extend and improve many other acceleration techniques.

Two examples of complementary techniques are partial  $k$ -space imaging [29] – which exploits conjugate symmetry in the Fourier transform of real images to sample only half of  $k$ -space – and the use of parallel receive arrays (multiple coils). Each can speed up MR image collection. Combined intelligently, the speed up from either methods multiplies the speed up from CS, producing an even faster hybrid imaging technique. Future research should ask how to best balance the speedups from each method, how they interact, and what the ultimate performance limits will be.

Many other fast imaging methods are closely related to CS, and can be extended using the CS framework. An excellent example is undersampling radial trajectories, mentioned above [9], [12]. This is successful exactly for the same reason that CS is successful. The point-spread function for undersampled radial sampling is incoherent (See Fig. 8c.). Undersampling artifacts contribute to an apparent noise level increase, but allow high-contrast objects like angiograms, to be reconstructed with high fidelity. The CS framework allows view streak artifacts to be rendered even more noise-like, and with nonlinear reconstruction this artifact can be largely eliminated from the reconstruction. Some of the work in applying the CS ideas to radial sampling has been presented by Chang et. al [36] Jung et. al [33] and Block et. al [35]

CS can also supplement existing approaches in dynamic imaging. There is a very long history of exploiting redundancy in the time series, either for imaging rapidly moving objects, such as the heart, or for imaging objects whose contrast is rapidly changing, such as in dynamic contrast uptake studies, and contrast angiography.

For rapidly moving objects like the heart, several methods attempt to reduce the Nyquist sampling requirements in  $k$ - $t$  space. One approach is UNFOLD [19] and a similar independently developed method by Willis [20], [21]. These methods attempt to match the temporal bandwidth of the dynamic series to allow greater spatial-frequency sampling. Aliasing is allowed in the individual images, and is suppressed by a temporal filter. Another approach is  $k$ - $t$  BLAST [27], which uses training data to learn and exploit

the spatio-temporal correlation to reconstruct high frame-rate dynamic images from reduced data. In comparison, CS uses a random sampling pattern to achieve the same end, without the need for training or prior knowledge of the spatio-temporal correlation. CS extensions to these ideas have been presented by Lustig et. al [32] and [34]

Considerable effort has also been devoted to developing methods for efficiently imaging objects where only the contrast of the image changes with time. These generally exploit the idea that the high spatial frequencies define the edges of the object, and are present throughout the study, or are slowly changing. The low spatial frequencies determine the contrast and appearance of the image, and must be tracked much more rapidly. An early example was KEYHOLE [22], which initially acquires a full resolution image of the object, followed by a time series of rapid, low resolution images. The low frequency data are combined with the original high spatial frequency data to produce a time series that has the spatial resolution of the original imaging, with the time resolution of the low-spatial resolution dynamic images. This works surprisingly well, but has significant limitations. For example, some part of the image may not show up at all until part way through the dynamic study, and won't be represented in the high spatial frequency data. This has been addressed by methods that continuously sample different k-space regions at different frequencies, so that the low frequencies are sampled much more rapidly, but all of k-space is acquired periodically. A particularly successful example is contrast angiography using TRICKS [25]. An extension of this is HYPR [28] which uses the undersampling characteristics of a radial acquisition that is interleaved to provide a complete acquisition over the duration of the study. The full reconstruction provides the high spatial resolution data of the spatial distribution of the signal, but has lost its dynamic information. Small subsets of the radial frames can be used with the spatial distribution constraint to provide high-temporal resolution dynamic contrast images, at full spatial resolution. This is a different perspective that achieves a result very similar to CS.

## VII. CONCLUSIONS

We have reviewed the requirements for CS and described their natural fit to MRI, emphasizing the different system-level factors that come into play in real applications.

We demonstrated four applications where CS improves on current imaging techniques. The concepts and the approaches we discussed should be useful to develop entirely new applications – perhaps solving problems that are intractable by current methods.

CS-MRI is in its infancy. Many crucial issues remain unsettled. For starters: optimizing sampling

trajectories; developing improved sparse transforms that are incoherent to the sampling operator; studying reconstruction quality in terms of clinical significance; improving the computation time of the reconstruction algorithms. The signal processing community has a major opportunity here: there are fascinating theoretical and practical research problems, promising substantial payoffs in improved medical care.

### VIII. ACKNOWLEDGMENTS

This project was supported by NIH grants: P41 RR09784, R01 HL074332, R01 HL075803 and GE healthcare. The authors would like to thank Walter Block for providing the data for the angiography example. The authors would also like to thank Peder Larson, Daeho Lee, Seung-Jean Kim and Yonit Lustig for their help with the manuscript.

### REFERENCES

- [1] E. Candès, J. Romberg, and T. Tao, "Robust uncertainty principles: Exact signal reconstruction from highly incomplete frequency information," *IEEE Transactions on Information Theory*, vol. 52, pp. 489–509, 2006.
- [2] D. Donoho, "Compressed sensing," *IEEE Transactions on Information Theory*, vol. 52, pp. 1289–1306, 2006.
- [3] G. Wright, "Magnetic resonance imaging," *Signal Processing Magazine, IEEE*, vol. 14, no. 1, pp. 56–66, Jan. 1997.
- [4] Z. P. Liang and P. C. Lauterbur, *Principles of Magnetic Resonance Imaging: A Signal Processing Perspective*. Picataway, NJ: IEEE Press, 1999.
- [5] M. A. Bernstein, F. K. King, and p. . X J Zhou; *Handbook of MRI pulse sequences*. Burlington, MA: Elsevier Academic Press, 2004.
- [6] E. M. Haacke, R. W. Brown, M. R. Thompson, and R. Venkatesan, *Magnetic Resonance Imaging: Physical Principles and Sequence Design*, 1st ed. New York: Wiley-Liss, 1999.
- [7] W. R. Nitz and P. Reimer, "Contrast mechanisms in MR imaging," *Eur Radiol*, vol. 9, no. 6, pp. 1032–46, 1999.
- [8] M. A. Bernstein, F. K. King, and p. . X J Zhou; *Handbook of MRI pulse sequences*. Burlington, MA: Elsevier Academic Press, 2004, ch. 16.
- [9] G. H. Glover and J. M. Pauly, "Projection reconstruction technique for reduction of motion effects in MRI," *Magn Reson Med*, vol. 28, pp. 275–289, 1992.
- [10] K. Scheffler and J. Hennig, "Reduced circular field-of-view imaging," *Magn Reson Med*, vol. 40, no. 3, pp. 474–480, 1998.
- [11] D. C. Peters, F. R. Korosec, T. M. Grist, W. F. Block, J. E. Holden, K. K. Vigen, and C. A. Mistretta, "Undersampled projection reconstruction applied to MR angiography," *Magn Reson Med*, vol. 43, no. 1, pp. 91–101, 2000.
- [12] A. V. Barger, W. F. Bloch, Y. Toropov, T. M. Grist, and C. A. Mistretta, "Time-resolved contrast-enhanced imaging with isotropic resolution and broad coverage using an undersampled 3d projection trajectory," *Magn Reson Med*, vol. 48, no. 2, pp. 297–305, 2002.
- [13] C. H. Meyer, B. S. Hu, D. G. Nishimura, and A. Macovski, "Fast spiral coronary artery imaging," *Magn Reson Med*, vol. 28, no. 2, pp. 202–213, 1992.

- [14] E. M. Haacke, R. W. Brown, M. R. Thompson, and R. Venkatesan, *Magnetic Resonance Imaging: Physical Principles and Sequence Design*, 1st ed. New York: Wiley-Liss, 1999, ch. 14.
- [15] J. I. Jackson, C. H. Meyer, D. G. Nishimura, and A. Macovski, "Selection of a convolution function for Fourier inversion using gridding," *IEEE Trans Med Imaging*, vol. 10, no. 3, pp. 473–478, 1991.
- [16] B. A. Chronik and B. K. Rutt, "Simple linear formulation for magnetostimulation specific to MRI gradient coils," *Magn Reson Med*, vol. 45, no. 5, pp. 916–919, 2001.
- [17] D. K. Sodickson and W. J. Manning, "Simultaneous acquisition of spatial harmonics (SMASH): Fast imaging with radiofrequency coil arrays," *Magn Reson Med*, vol. 38, no. 4, pp. 591–603, 1997.
- [18] K. P. Pruessmann, M. Weiger, M. B. Scheidegger, and P. Boesiger, "SENSE: Sensitivity encoding for fast MRI," *Magn Reson Med*, vol. 42, no. 5, pp. 952–962, 1999.
- [19] N. P. B. Madore, G.H. Glover, "Unaliasing by fourier-encoding the overlaps using the temporal dimension (UNFOLD), applied to cardiac imaging and fMRI," *Magn Reson Med*, vol. 42, no. 5, pp. 813–828, 1999.
- [20] N. P. Willis and Y. Bresler, "Optimal scan for time-varying tomography. I. Theoretical analysis and fundamental limitations." *IEEE Trans Image Process*, vol. 4, pp. 642–653, 1995.
- [21] ———, "Optimal scan for time-varying tomography. II. Efficient design and experimental validation." *IEEE Trans Image Process*, vol. 4, pp. 654–666, 1995.
- [22] J. J. van Valls, M. E. Brummner, W. T. Dixon, H. H. Tuithof, H. Engels, R. C. Nelson, B. M. Gerety, J. L. Chezmar, and J. A. Boer, "Keyhole method for accelerating imaging of contrast agent uptake." *J Magn Reson Imag*, vol. 3, pp. 671–675, 1993.
- [23] T. Parrish and X. Hu, "Continuous update with random encoding (CURE): a new strategy for dynamic imaging," *Magn Reson Med*, vol. 33, no. 3, pp. 326–336, Mar 1995.
- [24] M. Doyle, E. G. Walsh, G. G. Blackwell, and G. M. Pohost, "Block regional interpolation scheme for k-space (BRISK): a rapid cardiac imaging technique," *Magn Reson Med*, vol. 33, no. 2, pp. 163–170, Feb 1995, comparative Study.
- [25] F. R. Korosec, R. Frayne, T. M. Grist, and C. A. Mistretta, "Time-resolved contrast-enhanced 3D MR angiography," *Magn Reson Med*, vol. 36, no. 3, pp. 345–351, Sep 1996.
- [26] J. M. Hanson, Z. P. Liang, R. L. Magin, J. L. Duerk, and P. C. Lauterbur, "A comparison of RIGR and SVD dynamic imaging methods," *Magn Reson Med*, vol. 38, no. 1, pp. 161–167, Jul 1997, comparative Study.
- [27] J. Tsao, P. Boesiger, and K. P. Pruessmann, " $k$ - $t$  BLAST and  $k$ - $t$  SENSE: Dynamic MRI with high frame rate exploiting spatiotemporal correlations," *Magn Reson Med*, vol. 50, no. 5, pp. 1031–1042, 2003.
- [28] C. A. Mistretta, O. Wieben, J. Velikina, W. Block, J. Perry, Y. Wu, K. Johnson, and Y. Wu, "Highly constrained backprojection for time-resolved MRI," *Magn Reson Med*, vol. 55, no. 1, pp. 30–40, Jan 2006.
- [29] Z. P. Liang and P. C. Lauterbur, *Principles of Magnetic Resonance Imaging: A Signal Processing Perspective*. Picataway, NJ: IEEE Press, 1999, ch. 10.
- [30] M. Lustig, D. L. Donoho, and J. M. Pauly, "Sparse MRI: The application of compressed sensing for rapid MR imaging," *Magn Reson Med*, 2007, submitted.
- [31] M. Lustig, J. H. Lee, D. L. Donoho, and J. M. Pauly, "Faster imaging with randomly perturbed, undersampled spirals and  $|\ell|_1$  reconstruction," in *Proceedings of the 13th Annual Meeting of ISMRM*, Miami, 2005.
- [32] M. Lustig, J. M. Santos, D. L. Donoho, and J. M. Pauly, " $k$ - $t$  Sparse: High frame rate dynamic MRI exploiting spatiotemporal sparsity," in *Proceedings of the 13th Annual Meeting of ISMRM*, Seattle, 2006, p. 2420.

- [33] H. Jung, J. C. Ye, and E. Y. Kim, "Improved k-t BLAST and k-t SENSE using FOCUSS," *Phys Med Biol*, vol. 52, no. 11, pp. 3201–3226, Jun 2007.
- [34] J. C. Ye, S. Tak, Y. Han, and H. W. Park, "Projection reconstruction MR imaging using FOCUSS," *Magn Reson Med*, vol. 57, no. 4, pp. 764–775, Apr 2007.
- [35] K. T. Block, M. Uecker, and J. Frahm, "Undersampled radial MRI with multiple coils. Iterative image reconstruction using a total variation constraint," *Magn Reson Med*, vol. 57, no. 6, pp. 1086–1098, Jun 2007.
- [36] T.-C. Chang, L. He, and T. Fang, "Mr image reconstruction from sparse radial samples using bregman iteration," in *Proceedings of the 13th Annual Meeting of ISMRM*, Seattle, 2006, p. 696.
- [37] F. Wajer, "Non-cartesian mri scan time reduction through sparse sampling," Ph.D. dissertation, Delft University of Technology, 2001.
- [38] D. S. Taubman and M. W. Marcellin, *JPEG 2000: Image Compression Fundamentals, Standards and Practice*. Kluwer International Series in Engineering and Computer Science., 2002.
- [39] M. G. Strintzis, "A review of compression methods for medical images in PACS," *Int J Med Inform*, vol. 52, no. 1-3, pp. 159–165, Oct 1998, comparative Study.
- [40] E. L. Siegel and R. Khorasani, "To compress or not to compress: A compressed debate," *J Am Coll Radiol*, vol. 1, no. 12, pp. 981–983, Dec 2004.
- [41] D. Donoho, Y. Tsaig, I. Drori, and J.-L. Starck, "Sparse solution of underdetermined linear equations by stagewise orthogonal matching pursuit," *Technical Report, Department of Statistics, Stanford University*, 2006, preprint.
- [42] C.-M. Tsai and D. Nishimura, "Reduced aliasing artifacts using variable-density  $k$ -space sampling trajectories," *Magn Reson Med*, vol. 43, no. 3, pp. 452–458, 2000.
- [43] J. H. Lee, B. A. Hargreaves, B. S. Hu, and D. G. Nishimura, "Fast 3d imaging using variable-density spiral trajectories with applications to limb perfusion," *Magn Reson Med*, vol. 50, no. 6, pp. 1276–1285, 2003.
- [44] G. J. Marseille, R. de Beer, M. Fuderer, A. F. Mehlkopf, and D. van Ormondt, "Nonuniform phase-encode distributions for MRI scan time reduction," *J Magn Reson*, vol. 111, no. 1, pp. 70–75, 1996.
- [45] K. S. Nayak and D. G. Nishimura, "Randomized trajectories for reduced aliasing artifacts," in *Proceedings of the 6th Annual Meeting of ISMRM*, Sydney, 1998, p. 670.
- [46] A. Greiser and M. von Kienlin, "Efficient  $k$ -space sampling by density-weighted phase-encoding," *Magn Reson Med*, vol. 50, no. 6, pp. 1266–1275, Dec 2003.
- [47] D. Donoho, "For most large underdetermined systems of linear equations, the minimal  $\ell^1$  solution is also the sparsest solution," *Comm. Pure Appl. Math.*, vol. 59, pp. 797–829, June 2006.
- [48] L. Rudin, S. Osher, and E. Fatemi, "Non-linear total variation noise removal algorithm," *Phys. D*, vol. 60, pp. 259–268, 1992.
- [49] J.-L. Starck, M. Elad, and D. Donoho, "Image decomposition via the combination of sparse representation and a variational approach," *IEEE Trans. Image Proc.*, vol. 14, no. 10, pp. 1570–1582, 2005.
- [50] E. Candès and J. Romberg, "Practical signal recovery from random projections," *Caltech, Technical Report*, 2005, preprint.
- [51] E. Candès and F. Guo, "New multiscale transforms, minimum total variation synthesis: application to edge preserving image reconstruction," in *EURASIP*, vol. 82, no. 11, 2002, pp. 1519–1545.
- [52] M. Elad, B. Matalon, and M. Zibulevsky, "Coordinate and subspace optimization methods for linear least squares with non-quadratic regularization," *Journal on Applied and Computational Harmonic Analysis*, 2006, in Press.

- [53] J. Tropp and A. Gilbert, "Signal recovery from partial information by orthogonal matching pursuit. manuscript," *TBD*, vol. 00, pp. 00–00, 2005.
- [54] D. L. Parker, J. S. Tsuruda, K. C. Goodrich, A. L. Alexander, and H. R. Buswell, "Contrast-enhanced magnetic resonance angiography of cerebral arteries," *Investigative Radiology*, vol. 33, no. 9, pp. 560–572, Sept. 1998.
- [55] F. R. Korosec, R. Frayne, T. M. Grist, and C. A. Mistretta, "Time-resolved contrast-enhanced 3D MR angiography," *Magn Reson Med*, vol. 36, no. 3, pp. 345–351, Sep 1996.
- [56] M. Doyle, M. B. Scheidegger, R. G. Degraaf, J. Vermeulen, and G. M. Pohost, "Coronary artery imaging in multiple 1-sec breath holds," *Magnetic Resonance Imaging*, vol. 11, no. 1, pp. 3 – 6, 1993.
- [57] T. S. Sachs, C. H. Meyer, P. Irarrazabal, B. S. Hu, D. G. Nishimura, and A. Macovski, "The diminishing variance algorithm for real-time reduction of motion artifacts in MRI." *Magnetic Resonance in Medicine*, vol. 34, no. 3, pp. 412 – 22, 1995 1995.
- [58] M. Stuber, R. M. Botnar, P. G. Danias, D. K. Sodickson, K. V. Kissinger, M. V. Cauteren, J. D. Becker, and W. J. Manning, "Double-oblique free-breathing high resolution three-dimensional coronary magnetic resonance angiography," *Journal of the American College of Cardiology*, vol. 34, no. 2, pp. 524 – 531, Aug., 1999.
- [59] O. M. Weber, A. J. Martin, and C. B. Higgins, "Whole-heart steady-state free precession coronary artery magnetic resonance angiography." *Magnetic Resonance in Medicine*, vol. 50, no. 6, pp. 1223 – 8, December 2003.
- [60] J. M. Santos, C. H. Cunningham, M. Lustig, B. A. Hargreaves, B. S. Hu, D. G. Nishimura, and J. M. Pauly, "Single breath-hold whole-heart MRA using variable-density spirals at 3T," *Magnetic Resonance in Medicine*, vol. 55, no. 2, pp. 371–379, 2006.

LIST OF FIGURES

1 The magnetic fields used in MR imaging: The main homogeneous magnetic field  $B_0$  creates a net magnetization that precesses at a resonance frequency  $\frac{\gamma}{2\pi}B_0$ . The transverse rotating radio-frequency field  $B_1$  is used for exciting the magnetization. The gradient fields  $G$  (only  $G_x$  is illustrated) are used for spatial encoding. . . . . 26

2 Fourier spatial encoding. The temporal MRI signal directly samples the spatial frequency domain of the image. Gradient fields cause a linear frequency distribution across the image, which produces a linear phase accrual with time. The received signal samples are spatial frequencies of the image. The corresponding spatial frequencies are proportional to the gradient waveform area. The gradient is limited in amplitude,  $G_{\max}$ , and slew rate,  $S_{\max}$ , which are both system specific. . . . . 27

3 Image resolution is determined by the extent of the  $k$ -space that is covered. The supported field of view is determined by the sampling density. Violation of the Nyquist criteria causes the linear reconstruction to exhibit artifacts. The appearance of the artifact depends on the sampling. Equispaced sampling results in Coherent folding and irregular sampling results in incoherent aliasing. . . . . 28

4 Common sampling trajectories. Top, left to right: Cartesian 2D, Cartesian echo-planar, radial, spiral. Bottom left to right: Cartesian 3D, stack of radial, 3D radial, 3D stack of spirals . . . 29

5 Transform sparsity of MR images. Fully sampled images (left) are mapped by a sparsifying transform to a transform domain (middle); the several largest coefficients are preserved while all others are set to zero; the transform is inverted forming a reconstructed image (right). . . 30

6 MRI as a compressed sensing system: The user controls the gradient and RF waveforms which, in turn, control the phase of the pixels/voxels in the image. An RF coil receives the signal in an encoded form – samples in  $k$ -space. Careful crafting of the gradient waveforms allows for incoherent measurements of  $k$ -space. With an appropriate non-linear reconstruction enforcing sparsity, an image can be reconstructed. . . . . 31

7 Intuitive Procedure for Reconstruction from Undersampled Data. A sparse signal (1) is 8-fold undersampled in its 1D  $k$ -space domain (2). Equispaced undersampling results in signal aliasing (3a) that can not be recovered. Pseudo-random undersampling results in incoherent interference (3). Some strong signal components stick above the interference level, are detected and recovered by thresholding (4 and 5). The interference of these components is computed (6) and subtracted (7), thus lowering the total interference level and enabling recovery of weaker components . . . . . 32

8 Point Spread Functions (PSF) of various sampling trajectories. (a) Random lines in 2D (b) Random points in 2D, or cross-section of random lines in 3D (c) Radial (d) Uniform spirals (e) Variable density spirals (f) Variable density perturbed spirals . . . . . 33

9 Top left: Dynamic MRI is a multi-dimensional signal with two or three spatial coordinates and time as an additional dimension. Bottom left: Dynamic images have a sparse representation in an appropriate transform domain. Top right: Traditional  $k-t$  sequential sampling. Bottom right: Random ordering is an efficient way to incoherently sample the  $k-t$  space. . . . . 34

10 3D Contrast enhanced angiography. Top: Even with 10-fold undersampling CS can recover most blood vessel information revealed by Nyquist sampling; there is significant artifact reduction compared to linear reconstruction; and a significant resolution improvement compared to a low-resolution centric  $k$ -space acquisition. Bottom: The 3D Cartesian random undersampling configuration. . . . . 35

11	Single breath-hold whole heart coronary artery imaging. Left: the sequence diagram. Right: The incoherent artifacts of undersampled variable-density spirals appear as noiselike interference in the linear gridding reconstruction. These artifacts are suppressed in the CS reconstruction without compromising image quality . . . . .	36
12	CS exhibits suppression of aliasing artifacts over linear reconstruction from incoherent sampling, improved resolution over a low-resolution acquisition with the same scan time and a comparable reconstruction quality to a full Nyquist sampled set. . . . .	37
13	Dynamic imaging of quasi-periodic change. Top: Phantom experiment showing a reconstruction from 4-fold undersampling. Bottom: Dynamic acquisition of the heart motion showing a reconstruction from 7-fold undersampling. . . . .	38

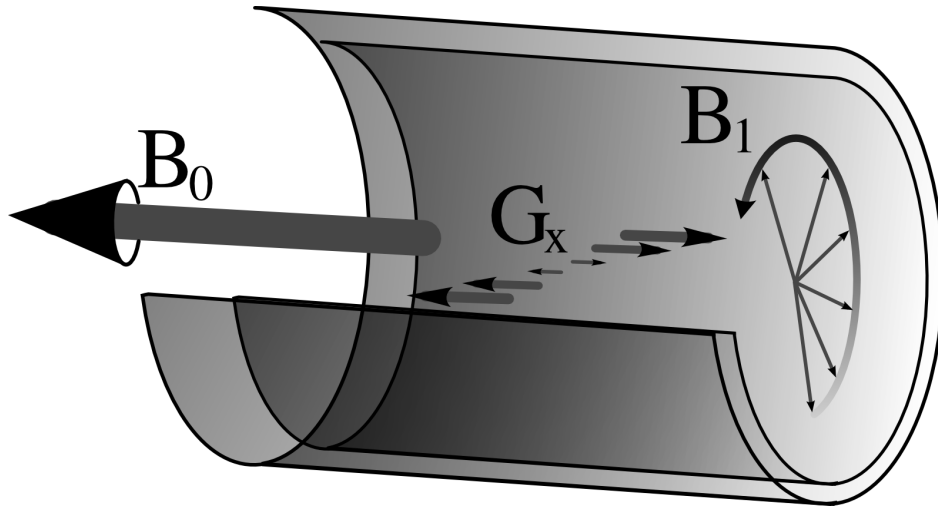


Fig. 1. The magnetic fields used in MR imaging: The main homogeneous magnetic field  $B_0$  creates a net magnetization that precesses at a resonance frequency  $\frac{\gamma}{2\pi}B_0$ . The transverse rotating radio-frequency field  $B_1$  is used for exciting the magnetization. The gradient fields  $G$  (only  $G_x$  is illustrated) are used for spatial encoding.

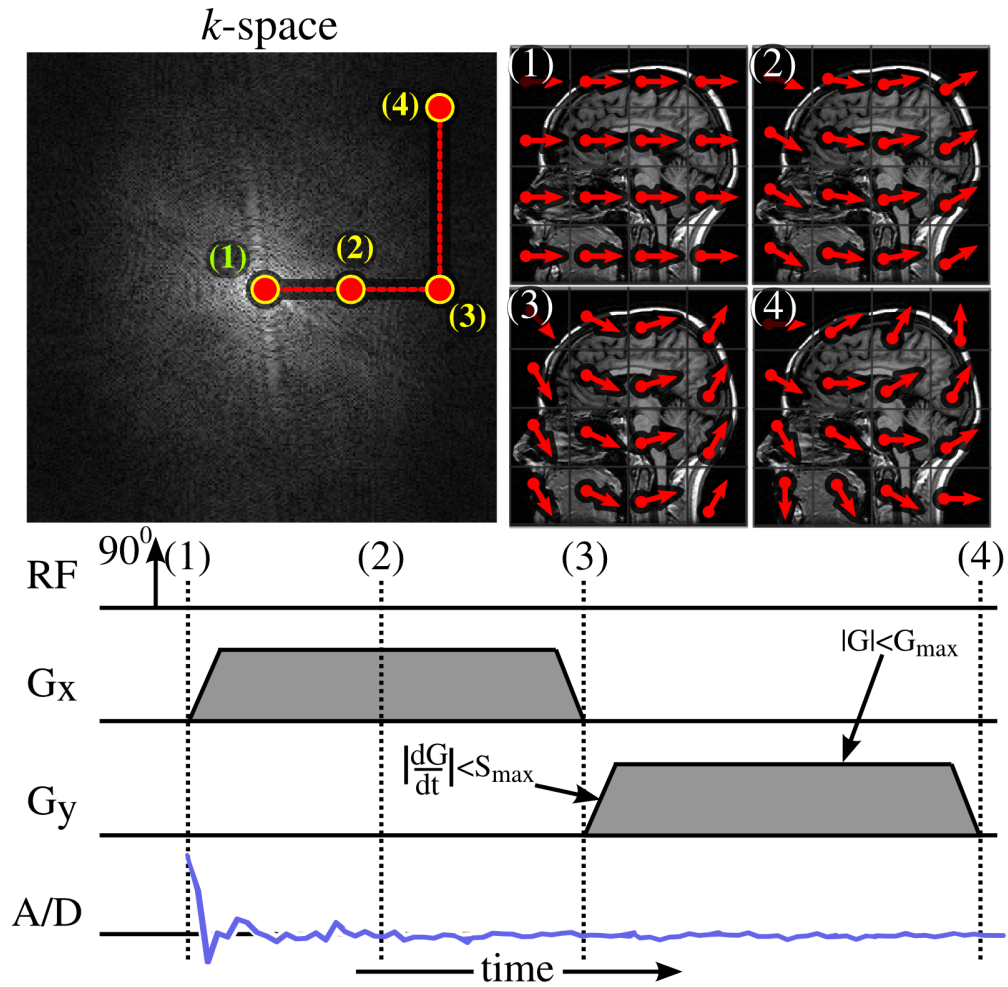


Fig. 2. Fourier spatial encoding. The temporal MRI signal directly samples the spatial frequency domain of the image. Gradient fields cause a linear frequency distribution across the image, which produces a linear phase accrual with time. The received signal samples are spatial frequencies of the image. The corresponding spatial frequencies are proportional to the gradient waveform area. The gradient is limited in amplitude,  $G_{max}$ , and slew rate,  $S_{max}$ , which are both system specific.

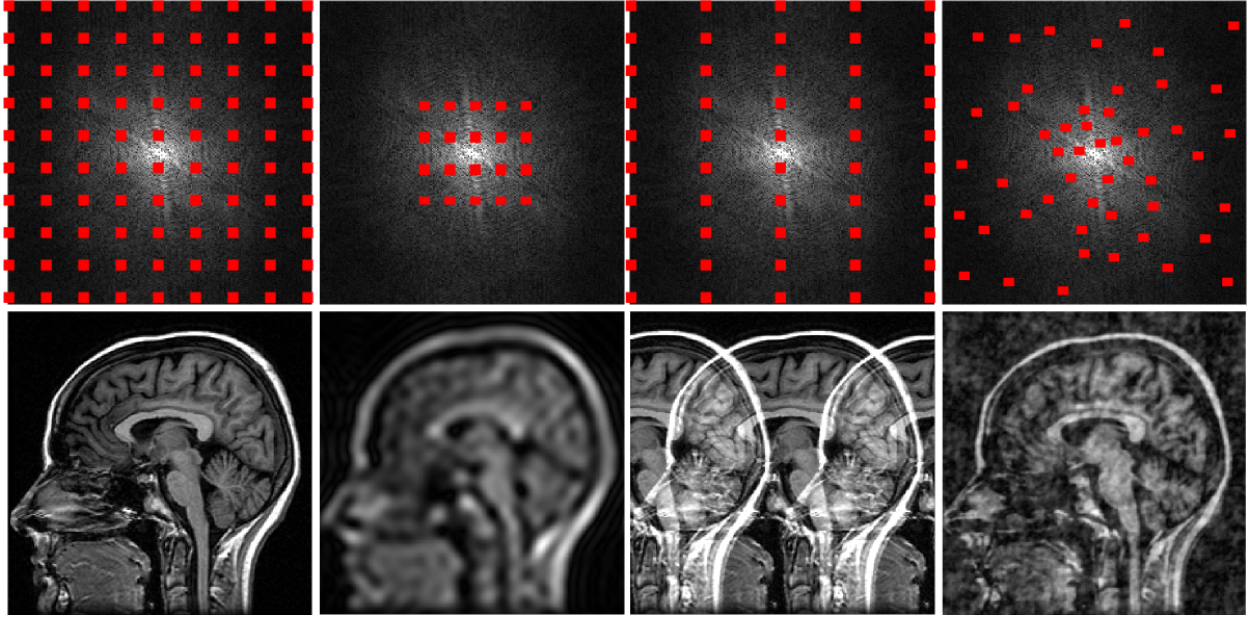


Fig. 3. Image resolution is determined by the extent of the  $k$ -space that is covered. The supported field of view is determined by the sampling density. Violation of the Nyquist criteria causes the linear reconstruction to exhibit artifacts. The appearance of the artifact depends on the sampling. Equispaced sampling results in Coherent folding and irregular sampling results in incoherent aliasing.

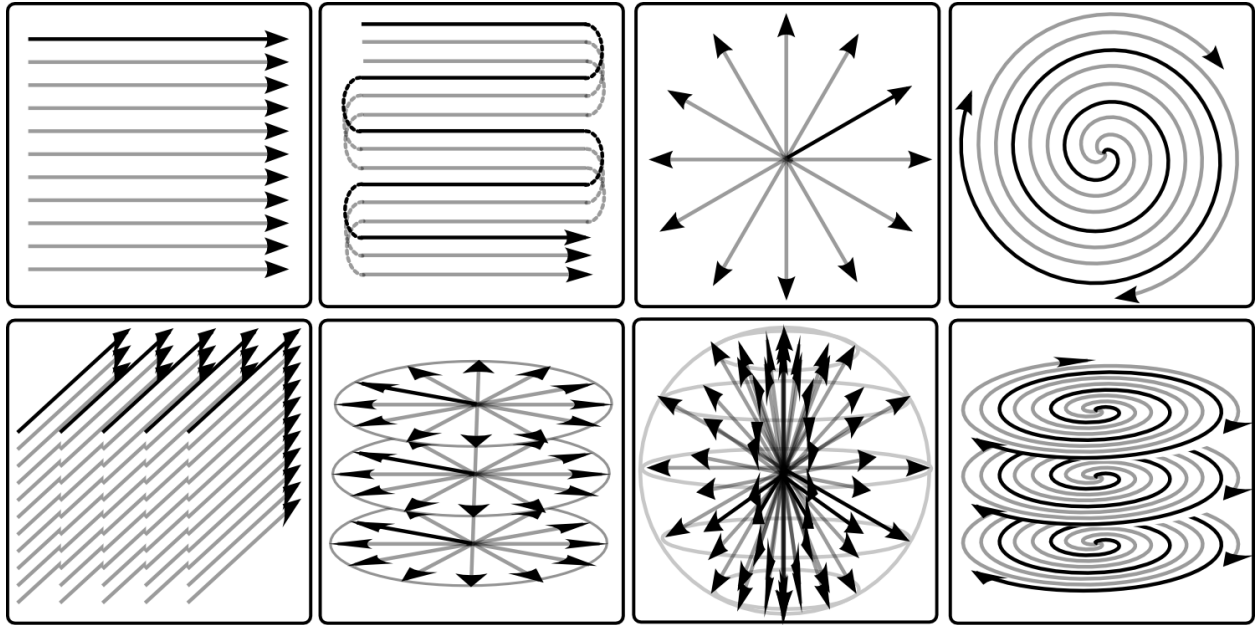


Fig. 4. Common sampling trajectories. Top, left to right: Cartesian 2D, Cartesian echo-planar, radial, spiral. Bottom left to right: Cartesian 3D, stack of radial, 3D radial, 3D stack of spirals

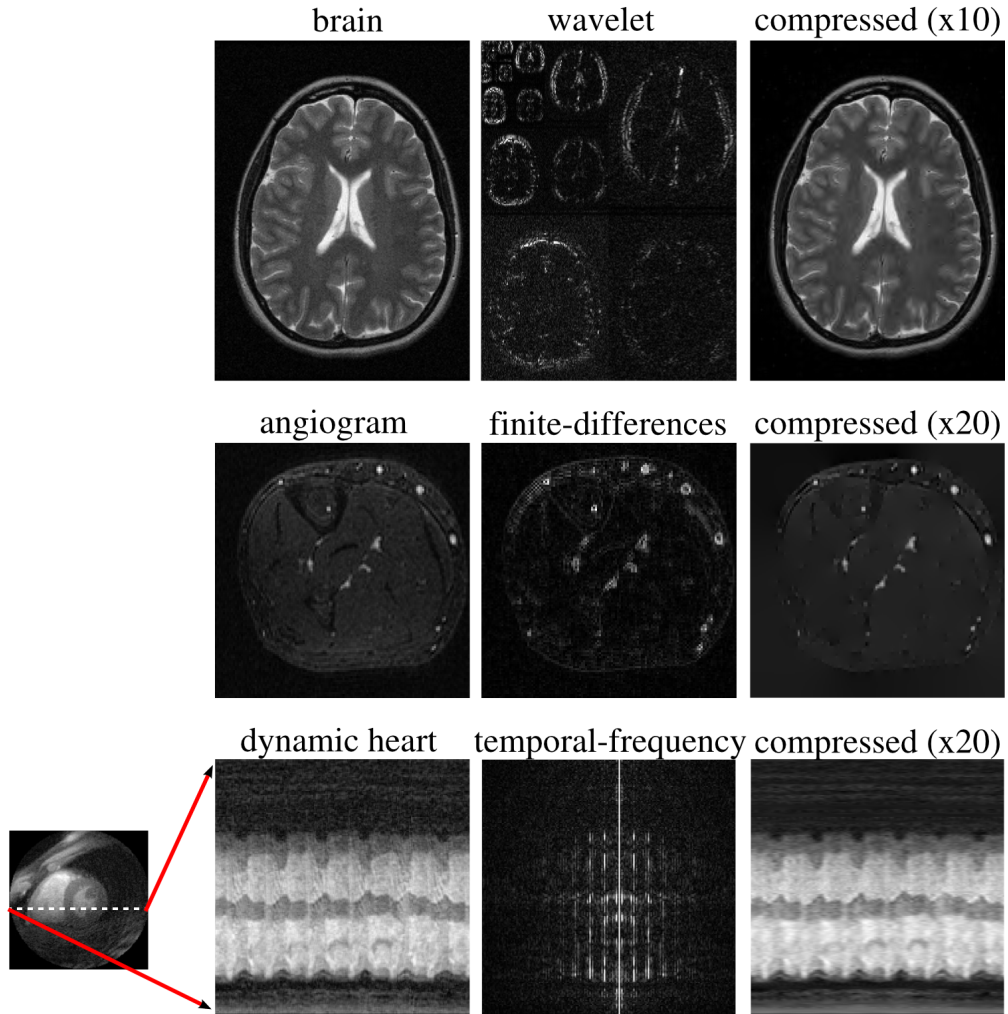


Fig. 5. Transform sparsity of MR images. Fully sampled images (left) are mapped by a sparsifying transform to a transform domain (middle); the several largest coefficients are preserved while all others are set to zero; the transform is inverted forming a reconstructed image (right).

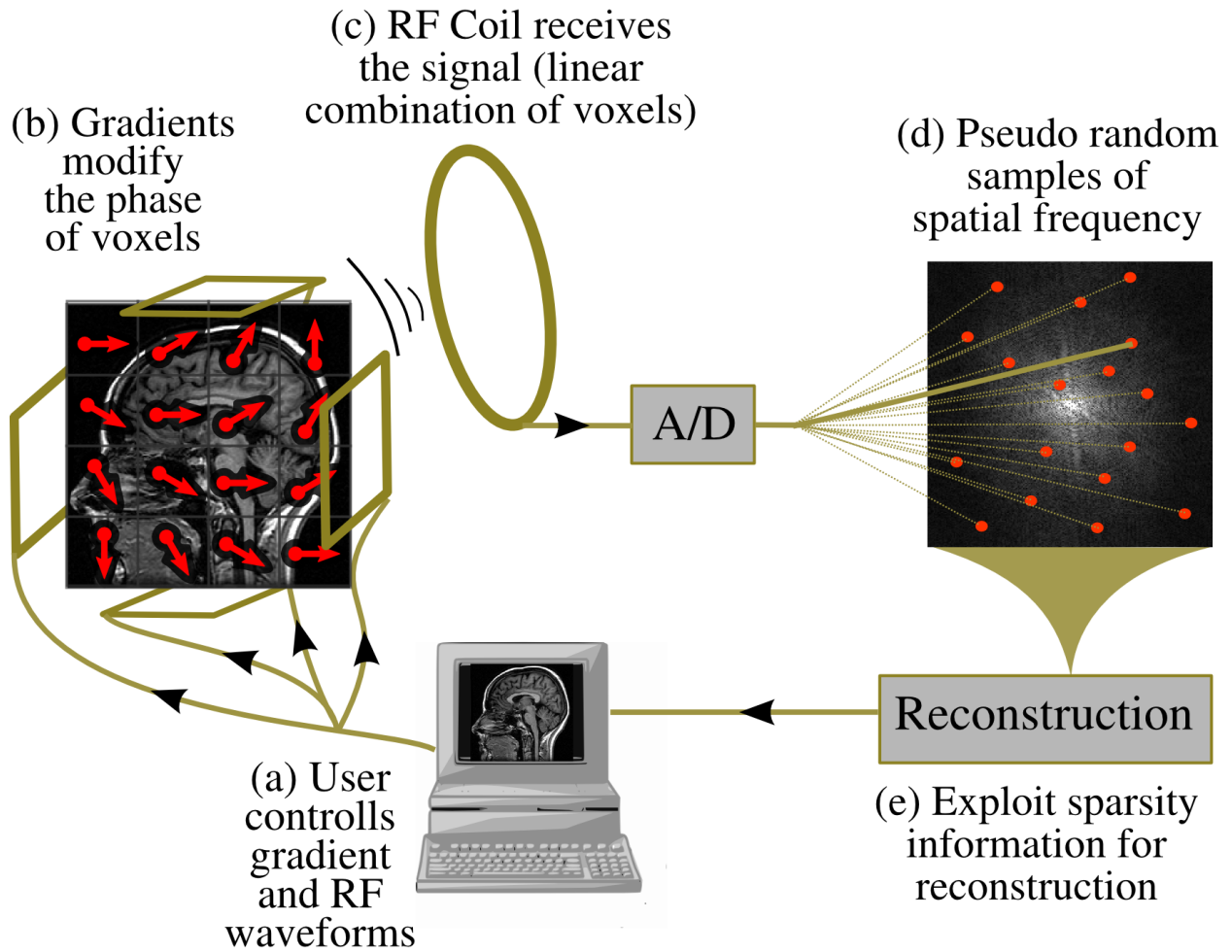


Fig. 6. MRI as a compressed sensing system: The user controls the gradient and RF waveforms which, in turn, control the phase of the pixels/voxels in the image. An RF coil receives the signal in an encoded form – samples in  $k$ -space. Careful crafting of the gradient waveforms allows for incoherent measurements of  $k$ -space. With an appropriate non-linear reconstruction enforcing sparsity, an image can be reconstructed.

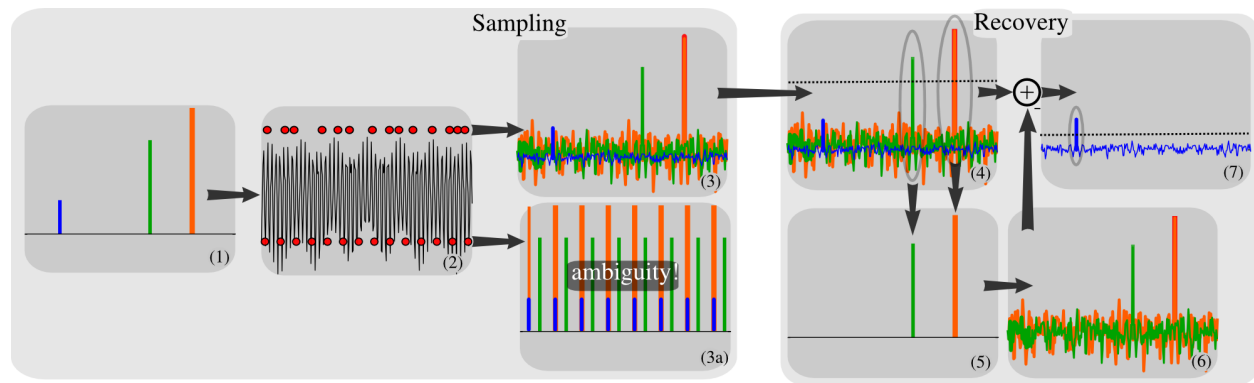


Fig. 7. Intuitive Procedure for Reconstruction from Undersampled Data. A sparse signal (1) is 8-fold undersampled in its 1D  $k$ -space domain (2). Equispaced undersampling results in signal aliasing (3a) that can not be recovered. Pseudo-random undersampling results in incoherent interference (3). Some strong signal components stick above the interference level, are detected and recovered by thresholding (4 and 5). The interference of these components is computed (6) and subtracted (7), thus lowering the total interference level and enabling recovery of weaker components

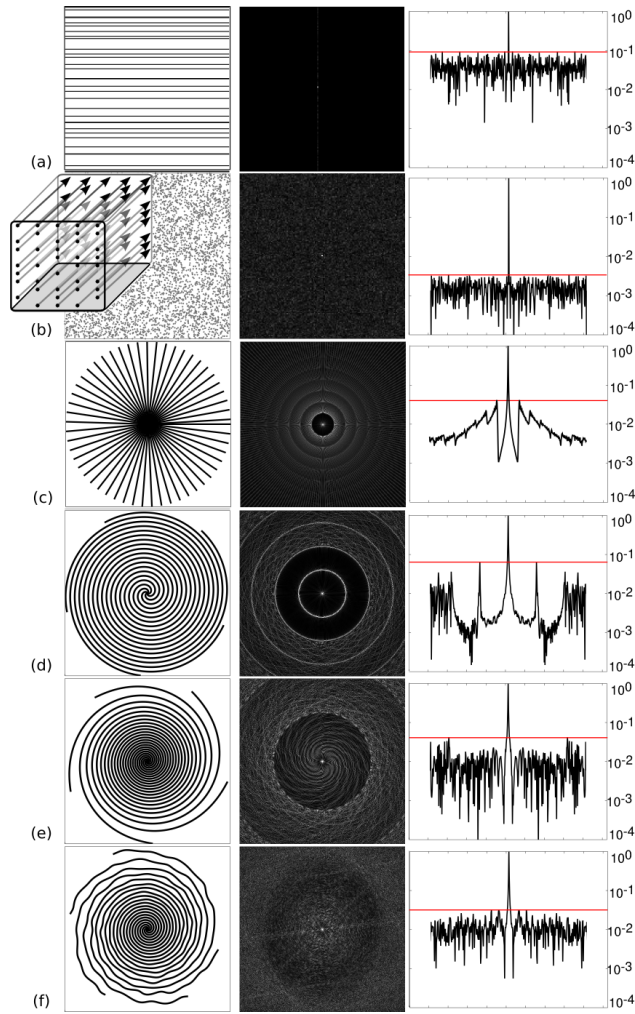


Fig. 8. Point Spread Functions (PSF) of various sampling trajectories. (a) Random lines in 2D (b) Random points in 2D, or cross-section of random lines in 3D (c) Radial (d) Uniform spirals (e) Variable density spirals (f) Variable density perturbed spirals

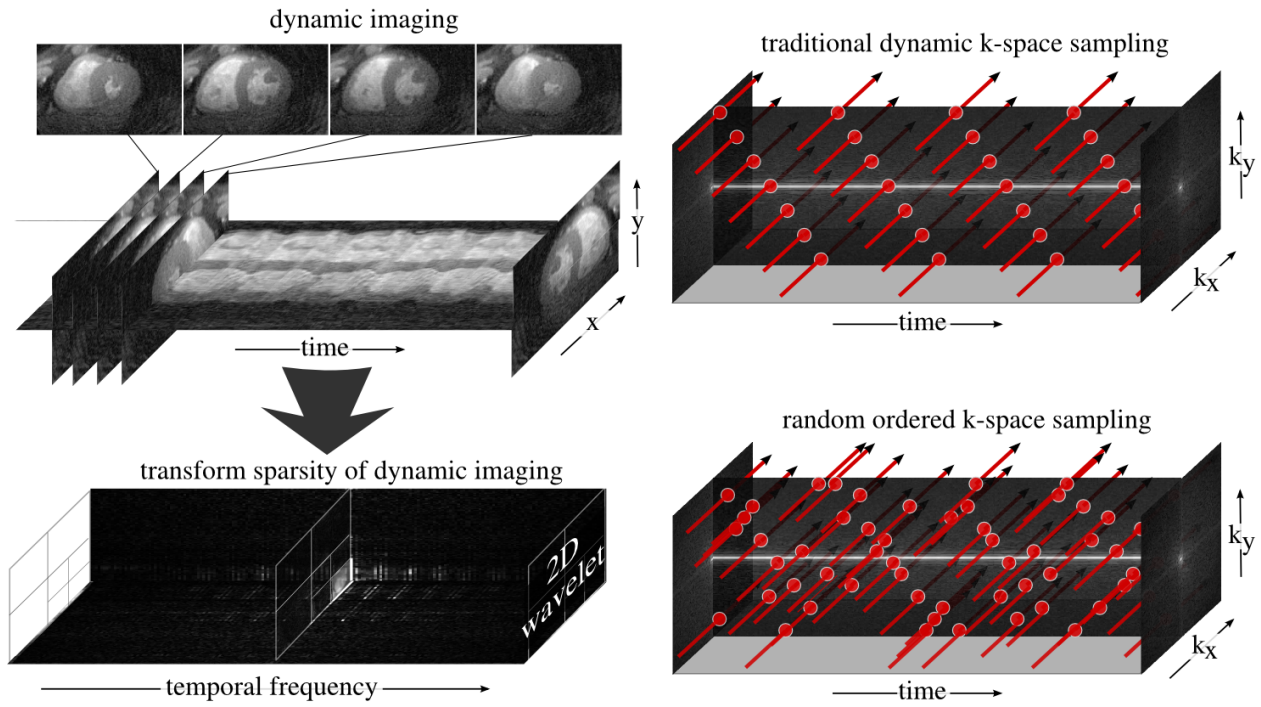
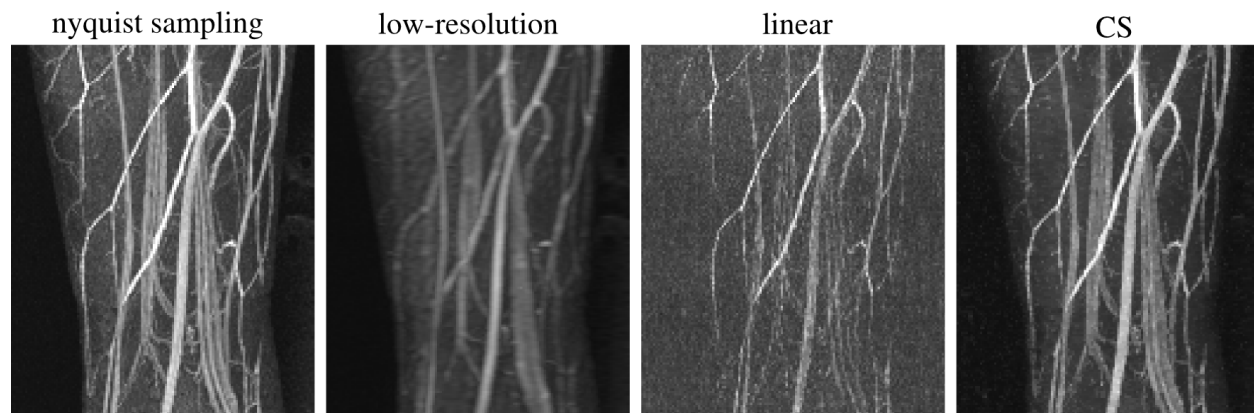


Fig. 9. Top left: Dynamic MRI is a multi-dimensional signal with two or three spatial coordinates and time as an additional dimension. Bottom left: Dynamic images have a sparse representation in an appropriate transform domain. Top right: Traditional  $k-t$  sequential sampling. Bottom right: Random ordering is an efficient way to incoherently sample the  $k-t$  space.



*3D Cartesian sampling configuration:*

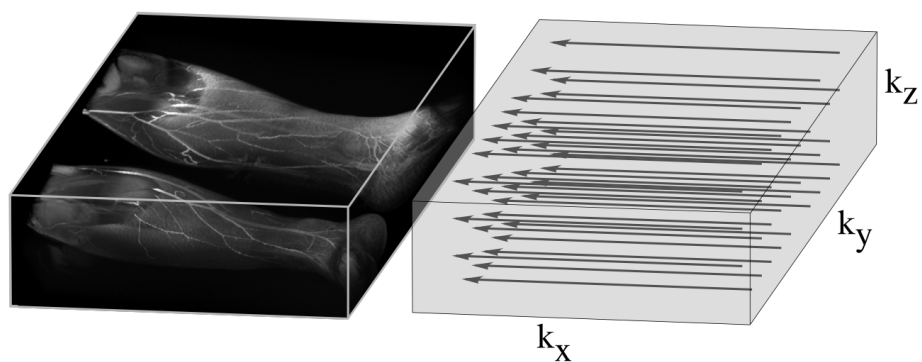


Fig. 10. 3D Contrast enhanced angiography. Top: Even with 10-fold undersampling CS can recover most blood vessel information revealed by Nyquist sampling; there is significant artifact reduction compared to linear reconstruction; and a significant resolution improvement compared to a low-resolution centric k-space acquisition. Bottom: The 3D Cartesian random undersampling configuration.

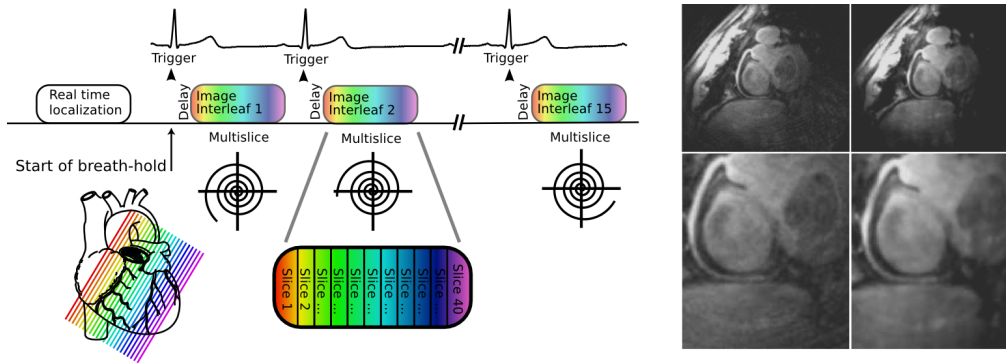
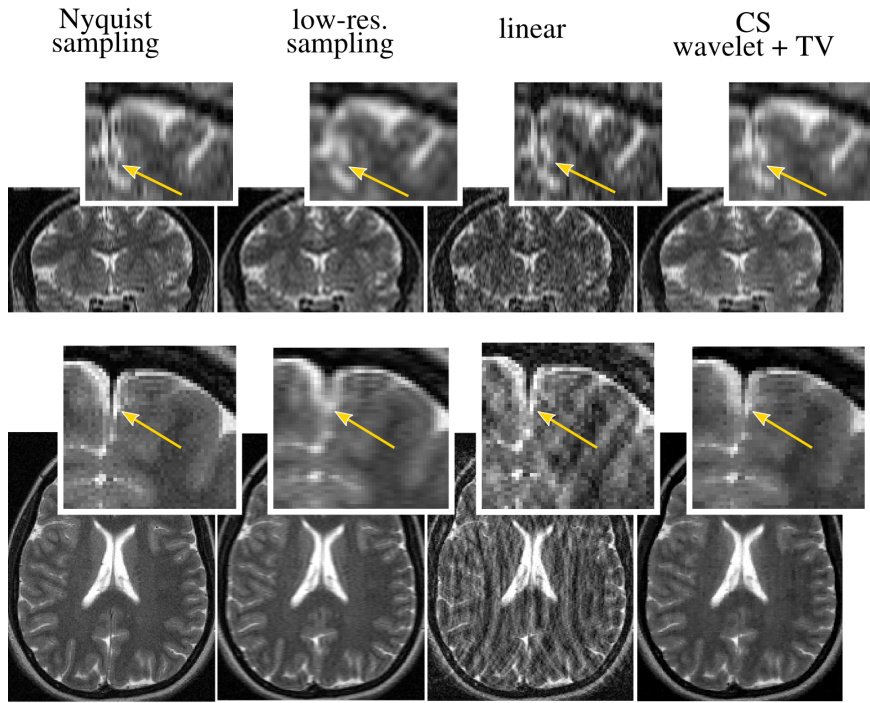


Fig. 11. Single breath-hold whole heart coronary artery imaging. Left: the sequence diagram. Right: The incoherent artifacts of undersampled variable-density spirals appear as noiselike interference in the linear gridding reconstruction. These artifacts are suppressed in the CS reconstruction without compromising image quality



*multi-slice 2D Cartesian sampling configuration:*

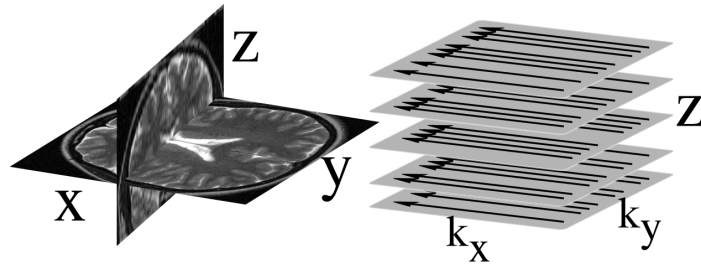


Fig. 12. CS exhibits suppression of aliasing artifacts over linear reconstruction from incoherent sampling, improved resolution over a low-resolution acquisition with the same scan time and a comparable reconstruction quality to a full Nyquist sampled set.

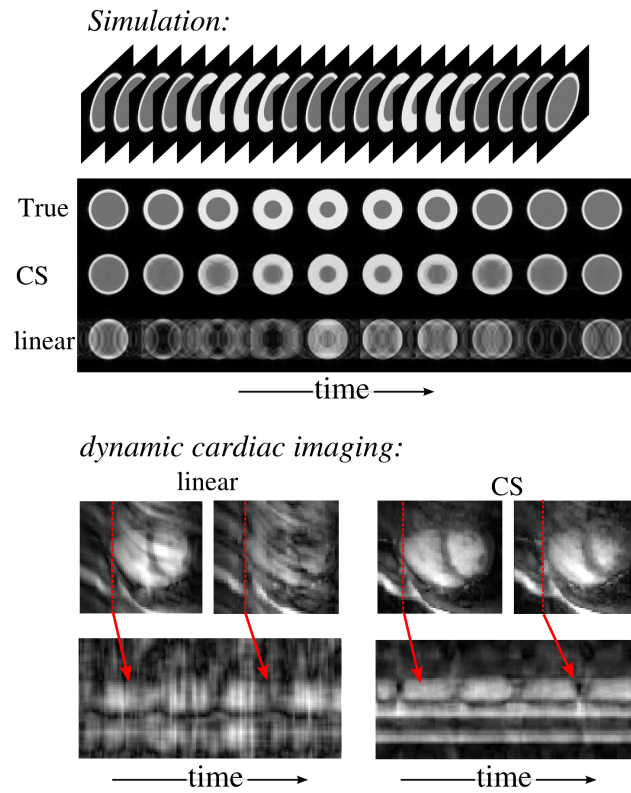


Fig. 13. Dynamic imaging of quasi-periodic change. Top: Phantom experiment showing a reconstruction from 4-fold undersampling. Bottom: Dynamic acquisition of the heart motion showing a reconstruction from 7-fold undersampling.